

The grating decomposition method: A new approach for understanding polarization-selective transient grating experiments. I. Theory

John T. Fourkas^{a)}

Department of Chemistry, Stanford University, Stanford, California 94305

Rick Trebino^{b)}

Combustion Research Facility, Sandia National Laboratories, Livermore, California 94551

M. D. Fayer

Department of Chemistry, Stanford University, Stanford, California 94305

(Received 11 March 1991; accepted 16 March 1992)

In this paper and the following paper (II) we introduce a new method of viewing transient holographic grating experiments in which the gratings are formed by laser beams of orthogonal linear or circular polarizations (or one of each). In this paper, we show that the two traditional methods of modeling these gratings, electric-field pictures and diagrammatic perturbation theory, may be augmented. We demonstrate that any grating can be decomposed into component intensity gratings that are related to the polarizations in its electric-field picture. Each of these component gratings may be analyzed separately (with or without diagrammatic perturbation theory), facilitating the incorporation of secondary effects (such as transport and heat deposition) into the grating calculation. The grating decomposition method (GDM) illuminates spatial structure that is not evident in standard perturbative calculations; it also provides a physical description that makes qualitative insights more readily obtainable, while at the same time making the electric-field approach rigorous and quantitative. Furthermore, the GDM reduces the complexity of many diagrammatic perturbation theory calculations. We also introduce effective two-interaction matrix elements (ETIMEs), which can be used to greatly simplify perturbative grating calculations. We show that ETIMEs, when considered in conjunction with the symmetry properties of the third-order susceptibility ($\chi^{(3)}$), can often be used to prove that some of the component gratings in a decomposition do not contribute to the signal and therefore need not be considered. In II, we apply this theory to two grating problems.

I. INTRODUCTION

Over the past two decades, four-wave mixing (FWM) techniques have become increasingly powerful tools for probing phenomena in all phases of matter.^{1,2} An important special case of FWM, the transient grating (TG),³ has proven useful in studying a multitude of processes. In the gas phase, velocity distributions, collisional excitation transfer,^{4,5} diffusional transport, and rates and cross sections for various sorts of collisions^{6,7} are among the phenomena that have been probed. Excited-state lifetimes,^{8,9} rotational rates,^{8,10} and the optical Kerr effect^{11,12} (OKE) are some of the processes that have been studied in liquids. Processes such as diffusion,¹³ molecular reorientations,¹⁴ and acoustic waves¹⁵ have been studied in various liquid-crystal phases. Solid-phase investigations have included excited-state dynamics,¹⁶ exciton transport in crystals,¹⁷ acoustic-wave propagation in bulk materials,¹⁸⁻²¹ and electron transport²² and other processes²³ in semiconductors. In addition, phase transitions,²⁴ porous materials,²⁵ and semiconductor-liquid interfaces²⁶ have been studied.

Although the transient grating is a versatile technique, TG data are not always simple to interpret, especially those arising from orientational gratings (a term that we will use to describe the general class of grating in which the polarization of the electric field changes along each fringe; an example of this is the linear polarization grating,²⁷⁻³¹ in which the excitation beams are of orthogonal linear polarizations). Historically, two approaches have been taken in the interpretation of orientational TG data. The first approach makes predictions based on the spatial dependence of the amplitude and polarization of the grating electric field.^{27,31-33} While this approach has the advantage of being simple and intuitive, it provides little calculational power and can lead to false insights.

The other approach that has been used to understand TG experiments and FWM in general³⁴⁻⁴¹ is the density-matrix formalism, usually in the form of diagrammatic perturbation theory (DPT), although Wherrett, Smirl, and Boggess have used iterative density-matrix techniques to model linear polarization gratings.²⁹ In this formalism, Feynman diagrams are used to depict integrals that describe the couplings of the material states by radiation fields and the evolution of these material states in between the field interventions. A weakness of this theory as it is usually applied to orientational TG experiments, however, is that spatial information about the excitation processes is buried in

^{a)} Present address: Department of Chemistry and Biochemistry, University of Texas at Austin, Austin, TX 78712.

^{b)} Supported by the U.S. Department of Energy, Office of Basic Energy Sciences, Chemical Sciences Division.

the mathematics of the calculation and is not available in a form that provides physical insight. This information can be essential to the understanding and calculation of orientational gratings and their decays for several reasons. First, decay constants must be added in a completely *ad hoc* manner. For instance, in the following paper⁴² (hereafter referred to as II) we discuss gratings of gas-phase sodium atoms. In this system, the decay constants for both linear polarization gratings and linear intensity gratings (in which the excitation beams have parallel polarizations) are calculationally indistinguishable, even though the experimentally observed decay constants differ greatly.^{6,7} Such differences arise because of the different spatial dependences of the excitation processes in each experiment. Second, DPT only formally treats two processes: the coherent coupling of material states via radiation fields and the subsequent decays of these coherences. Secondary effects such as thermal gratings¹⁹ or molecular alignment (through the nuclear optical Kerr effect,³² for instance) cannot be directly treated within the formalism, even though they may be major contributors to grating signals. It is difficult to extend this theory to treat such processes without understanding the spatial nature of the excitation process.

In this paper we use DPT to show rigorously that it is possible, through a change of basis set, to transform calculations of orientational gratings into sums of linear and circular intensity-grating calculations; we call this system the grating decomposition method (GDM). The electric field of each component intensity grating is of one polarization but is spatially modulated in amplitude; in this manner, spatial information is restored to the calculation in a form in which it can be used readily. Although we develop the GDM within the framework of DPT, the results derived are general properties of the third-order susceptibility ($\chi^{(3)}$), and the GDM is therefore valid no matter what method is used to calculate $\chi^{(3)}$. We further show that there is a direct connection between the electric-field pictures of orientational gratings and the decompositions associated with these gratings; thus, electric-field pictures and $\chi^{(3)}$ can provide great physical insight and simplify calculations when used in concert.

We also introduce effective two-interaction matrix elements (ETIMEs), which can greatly simplify perturbative grating calculations because much of the necessary summation is done in advance. Finally, we show that the symmetry properties of the ETIMEs and of $\chi^{(3)}$ can be used to predict which gratings in a decomposition do not need to be considered because of canceling contributions. We demonstrate the use of these symmetry properties in linear polarization-grating calculations in isotropic media. In II, we illustrate applications of the GDM to general and specific grating calculations.

II. BACKGROUND

In the most general FWM experiment, three input beams (of frequencies ω_1 , ω_2 , and ω_3 and polarizations η_1 , η_2 , and η_3 , respectively) enter the sample at times t_1 , t_2 , and t_3 ; the signal beam emerges at frequency ω_s , polarization η_s , and time t_s . In a TG experiment, beams 1 and 2 (the “excita-

tion” beams) are time coincident and usually (but not necessarily⁴³) of the same frequency; these beams make some angle θ with each other, and the resultant interference pattern creates a grating within the sample. Beam 3 (the “probe” beam), which may have a different frequency than the first two beams, arrives some time later and diffracts off of the grating. The diffracted portion of the probe beam forms the signal beam. (In another variety of induced-grating experiment, the laser pulses are all time coincident and the frequency of one or more of the beams is scanned instead of the probe pulse delay; the formalism developed in this paper applies equally well to this frequency-domain grating technique, although we will concentrate on the applications to TG experiments.)

Table I lists the five distinct combinations of excitation beam polarizations that may be used in creating gratings, and the types of grating each combination creates (other grating configurations are possible, but these may be reduced to linear combinations of those listed). Figure 1 shows the spatial variation of the electric fields for each of these gratings. The first variety of grating, the linear intensity grating (which we will henceforth call an intensity grating), is the most common. In this sort of grating, the excitation beams have parallel linear polarizations (which we have represented by x,x). The probe beam polarization is generally also linear, and the signal beam has the same polarization as the probe beam. As can be seen in Fig. 1(a), the intensity grating arises from an optical interference pattern between the two excitation beams. This intensity pattern interacts linearly with the medium and causes a sinusoidal ($1 + \cos \theta$) variation in its index of refraction; this variation in turn acts as a grating and diffracts the probe beam. (If the interaction with the medium is not linear, as in the case of two-photon absorption, the initial grating has a form other than $1 + \cos \theta$; such nonlinear interactions can be treated by extension of the treatment described here, and will not be discussed further in this paper.)

The second variety of grating that we consider is the linear polarization grating (which we will henceforth call a polarization grating). In this grating, the excitation beams are cross polarized (in this case we have chosen x,y). The probe beam (and therefore the signal beam) is again generally linearly polarized, but the angle between the probe and signal polarizations may range anywhere from 0° to 90° (depending on the choice of probe beam polarization and the relative strengths of the various relevant off-diagonal elements of the response tensor of the medium). Figure 1(b)

TABLE I. Types of induced grating.

Type of grating	Beam polarizations	Example
Linear intensity	Parallel linear	x,x
Linear polarization	Orthogonal linear	x,y
Circular intensity	Identical circular	r,r
Circular polarization	Opposite circular	r,l
Mixed	Circular and linear	r,x

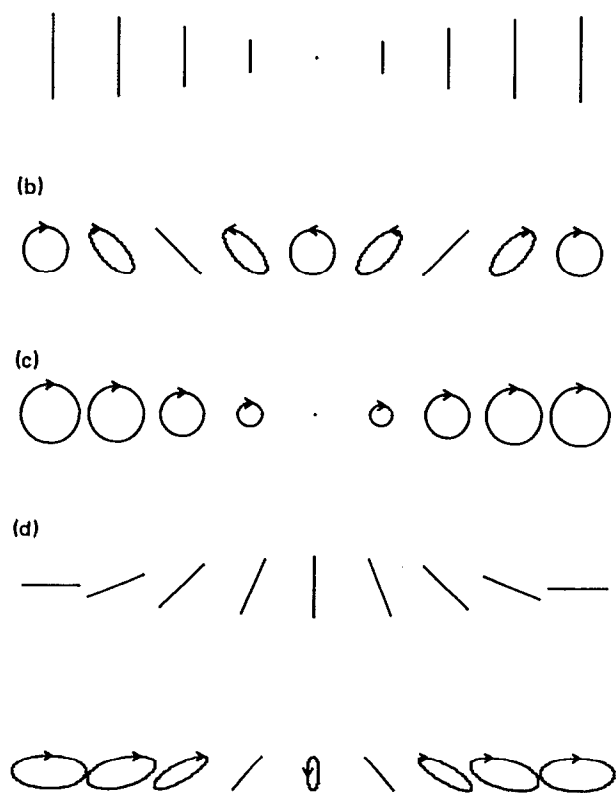


FIG. 1. Spatial dependence of electric field for one fringe of (a) linear intensity grating, (b) linear polarization grating, (c) circular intensity grating, (d) circular polarization grating, and (e) "mixed" grating.

shows how the electric field varies along one fringe of a polarization grating; note that the electric field changes in polarization but not in magnitude across a fringe (as opposed to the electric field in an intensity grating, which changes in magnitude but not in polarization). The polarization alternates from right circular to linear ($x - y$) to left circular to linear ($x + y$) and then back to right circular, with elliptical polarizations interspersed between the linear and circular polarizations. Since the e field changes in polarization along each grating fringe spacing, the polarization grating is a form of orientational grating.

The next two types of gratings are the circular analogs of the intensity and the polarization gratings (in Table I and elsewhere we denote right and left circular polarizations by r and l , respectively). In a circular intensity grating [Fig. 1(c)] the excitation beams have identical circular polarizations, whereas in a circular polarization grating [Fig. 1(d)] the excitation beams are of opposite circular polarizations. Finally, the last variety of grating consists of one circularly polarized excitation beam and one linearly polarized excitation beam [in Fig. 1(e) we show r and x polarizations]; we have termed this a "mixed" grating.

It is possible, given these pictures, to understand many of the factors that contribute to grating decays. Anything that causes the sinusoidal modulations that make up the induced gratings to lose amplitude will cause the signal to de-

cay. For instance, diffusion across a grating will progressively wash out the grating. Similarly, any population relaxation (such as excited-state decay) will usually cause the grating to decay. Orientational gratings [Figs. 1(b) and 1(d)] formed in liquids by excitation of randomly oriented molecules with well-defined transition-dipole directions will decay completely by rotational diffusion of the molecules; however, rotational diffusion will cause an intensity-grating signal to decay only partially or not at all (when the angle between the excitation and probe polarization is the magic angle²⁷).

The electric-field pictures also give insight as to the preparation of populations in various regions of a grating. This insight can be valuable in understanding grating signals, especially those arising from orientational gratings. For instance, many atoms and molecules have different selection rules for excitation by circularly polarized and linearly polarized light; in such cases, the populations prepared in different regions of a polarization grating can have vastly different properties.

This pictorial method facilitates an understanding of the excitation and decay processes that contribute to grating signals, although the actual calculation of grating decays from these pictures may be quite involved. While the effect of transport on any sort of grating is straightforward to calculate using this approach, there are many subtleties that can make it difficult to predict anything more than the qualitative nature of other orientational grating decay processes. It is desirable to have a more detailed mathematical theory of TG experiments that retains both the calculational ability of standard DPT and the qualitative insights of the spatial electric-field grating descriptions.

III. GRATING DECOMPOSITION

In this section we develop the mathematical basis of the GDM. We start by expressing the TG third-order polarization in a compact form consisting of what we call field products. The field product notation is intended to emphasize the electric fields involved in a TG experiment (rather than the material energy states). The mathematical properties of the field products will then allow us to use standard polarization relations to reexpress the field product for the excitation beams in any TG experiment as a sum of intensity-grating field products.

In a FWM experiment, the three incident fields interact through the third-order nonlinear susceptibility ($\chi^{(3)}$) of the medium; multiplying $\chi^{(3)}$ by the electric fields of the incident beams gives the third-order electric polarization of the material ($\rho^{(3)}$). The signal is derived by multiplying $\rho^{(3)}$ by its complex conjugate and then integrating over all observation times. A common scheme for calculating $\rho^{(3)}$ is DPT, making use of the material density matrix. $\rho^{(3)}$ is derived by summing three-dimensional time-ordered integrals that consider the coherent coupling of material states by the radiation fields and the evolution of the material-state coherences between these interactions. There are 48 separate sets of integrals to be evaluated in the calculation of $\rho^{(3)}$ for the most general FWM experiment; these integrals must then be

summed over all of the relevant material states and averaged over the distribution of molecular orientations.³⁶⁻⁴¹ It is common to use double-sided Feynman diagrams or energy-level "ladder" diagrams as an aid in deriving and evaluating the necessary integrals in a given problem. Time-ordering constraints (i.e., only allowing the probe beam to interact with the material after both of the excitation beams have interacted with the material, or equivalently, only considering $\rho^{(3)}$ at delay times greater than the duration of the pulses used in the experiment) and the application of the rotating-wave approximation limit the number of these diagrams that need be considered in the analysis of a TG experiment to at most four.³⁹ These four general processes are shown in double-sided Feynman diagram form in Fig. 2 and in ladder diagram form in Fig. 3.

These diagrammatic methods provide a powerful tool for calculating TG signals. However, even with the simplifications afforded by the diagrammatic approach, such calculations can be quite involved. Our purpose here is to deal only with one piece of these calculations, the electric-field polarizations and transition-dipole matrix elements. The polarizations and matrix elements are important factors in all induced-grating experiments, and together they may provide useful and general insights into orientational gratings. Thus we express $\rho^{(3)}$ as a sum of terms of the form

$$\langle c | \eta_j \cdot \mathbf{r} | a \rangle \langle b | \eta_k^* \cdot \mathbf{r} | c \rangle \langle d | \eta_m \cdot \mathbf{r} | b \rangle \langle a | \eta_n^* \cdot \mathbf{r} | d \rangle \times g(E_1, E_2^*, E_3, t_1, t_2, t_3, t, t_{\text{ob}}), \quad (1)$$

where $|a\rangle$, $|b\rangle$, $|c\rangle$, and $|d\rangle$ are material states (we use the convention in this paper that material-state energy increases

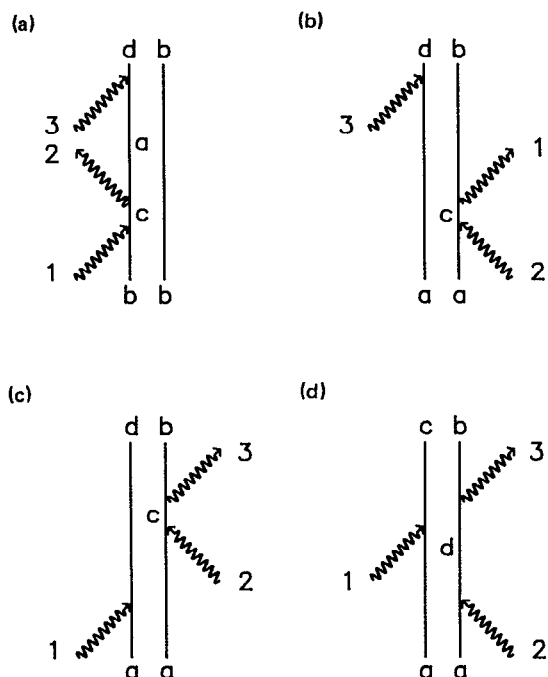


FIG. 2. The four processes that are important in transient grating calculations, expressed as double-sided Feynman diagrams.

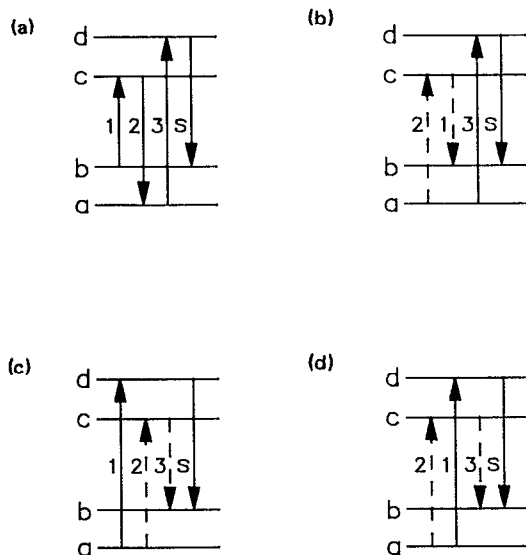


FIG. 3. The four processes that are important in transient grating calculations, expressed as ladder diagrams. The solid arrows represent ket-side field interventions, while the dashed arrows represent bra-side field interventions.

from $|a\rangle$ to $|d\rangle$), η_q is the polarization and phase of field q , and g is a complicated function of electric fields, intervention times, the probe delay time (t), and the observation time (t_{ob}); we leave g in general form for now. Note that two of the field polarizations are expressed as complex conjugates, for reasons that are made clear later. The total third-order polarization is the sum of these terms over all relevant material states and Feynman diagrams. The matrix elements in Eq. (1) do not have a specific time ordering associated with them; however, all of the products of matrix elements that we use from now on will be implicitly time ordered unless otherwise noted.

We can now introduce a new notation that concentrates on the polarizations of the light fields and not on the material energy levels. The dot product in each matrix element is represented solely by the polarization of the electric field involved (including an asterisk for conjugate fields). Time-coincident fields are placed in curly brackets; we call these sets of brackets field products. Square brackets are placed around a set of field products that constitutes a complete experiment. We thus write for a general induced-grating experiment

$$\langle c | \eta_j \cdot \mathbf{r} | a \rangle \langle b | \eta_k^* \cdot \mathbf{r} | c \rangle \langle d | \eta_m \cdot \mathbf{r} | b \rangle \langle a | \eta_n^* \cdot \mathbf{r} | d \rangle = [\{ \eta_j, \eta_k^* \} \{ \eta_m, \eta_n^* \}]. \quad (2)$$

The first field product in this equation contains the time-coincident excitation fields and the second field product contains the time-coincident probe and signal field. In general, we will only be concerned with the excitation fields, since we are interested in the spatial properties of the gratings that we create; however, it is also useful at times to consider the probe and signal polarizations.

Because the dot products in the matrix elements are ses-

quilinear (i.e., they follow a law analogous to the distributive law for multiplication), the polarizations in the field products (as well as any combinations of field products) are as well. In other words, if $\eta_j = \eta_r + \eta_s$, then

$$[\{\eta_r, \eta_s^*\} \{\eta_m, \eta_n^*\}] = [\{\eta_r, \eta_s^*\} \{\eta_m, \eta_n^*\}] + [\{\eta_s, \eta_s^*\} \{\eta_m, \eta_n^*\}]. \quad (3)$$

In fact, we can express any electric-field polarization as a sum of two other polarizations. A complete set of polarization relationships is given in Table II. Note that the phases of the polarizations are introduced by expressing the polarizations as having both real and imaginary parts. We have also introduced two new linear polarizations; **p** (plus) and **m** (minus), that are at $+45^\circ$ and -45° , respectively.

Using the relations in Table II, we can decompose the excitation fields for each of the five varieties of grating we have discussed; Table III shows examples of some of the more useful of these decompositions. For each type of grating, we can find a decomposition that corresponds to the electric-field picture for that grating. The important point is that it is always possible to decompose a grating into a superposition of intensity gratings, each of which has a single electric-field polarization and an intensity modulation with the period of the fringe spacing. We will discuss the decomposition of the polarization grating in some detail, and a similar process may be followed for each of the other sorts of grating.

We start out by writing, for the excitation polarizations,

$$\{\mathbf{x}, \mathbf{y}^*\} = (i/2) (\{\mathbf{l}, \mathbf{r}^*\} - \{\mathbf{r}, \mathbf{l}^*\} + \{\mathbf{r}, \mathbf{r}^*\} - \{\mathbf{l}, \mathbf{l}^*\}). \quad (4)$$

Similarly, we can show that

$$\{\mathbf{l}, \mathbf{r}^*\} - \{\mathbf{r}, \mathbf{l}^*\} = -i(\{\mathbf{x}, \mathbf{y}^*\} + \{\mathbf{y}, \mathbf{x}^*\}) = i(\{\mathbf{m}, \mathbf{m}^*\} - \{\mathbf{p}, \mathbf{p}^*\}). \quad (5)$$

Combining these results, we find

$$\{\mathbf{x}, \mathbf{y}^*\} = (i/2) (\{\mathbf{r}, \mathbf{r}^*\} + i\{\mathbf{m}, \mathbf{m}^*\} - \{\mathbf{l}, \mathbf{l}^*\} - i\{\mathbf{p}, \mathbf{p}^*\}). \quad (6)$$

The coefficient in front of each term in this expression ($+1$, i , -1 , or $-i$) is its complex spatial phase. Equation (6) is equivalent to the polarization identity for inner products in functional analysis.⁴⁴ Note that this does not necessarily imply that field products are inner products, however; the sesquilinearity of matrix elements is enough to ensure that field

TABLE III. Useful grating decompositions.

Type of grating	Example decomposition
Linear polarization	$\{\mathbf{x}, \mathbf{y}^*\} = \frac{1}{2}(\{\mathbf{p}, \mathbf{p}^*\} + i\{\mathbf{r}, \mathbf{r}^*\} - \{\mathbf{m}, \mathbf{m}^*\} - i\{\mathbf{l}, \mathbf{l}^*\})$
Circular polarization	$\{\mathbf{r}, \mathbf{l}^*\} = \frac{1}{2}(\{\mathbf{x}, \mathbf{x}^*\} + i\{\mathbf{p}, \mathbf{p}^*\} - \{\mathbf{y}, \mathbf{y}^*\} - i\{\mathbf{m}, \mathbf{m}^*\})$
Mixed	$\{\mathbf{r}, \mathbf{x}^*\} = (1/\sqrt{2})(\{\mathbf{x}, \mathbf{x}^*\} + i\{\mathbf{y}, \mathbf{x}^*\}) = (1/\sqrt{2})(\{\mathbf{x}, \mathbf{x}^*\} + (i/2)\{\mathbf{m}, \mathbf{m}^*\} + i\{\mathbf{r}, \mathbf{r}^*\} - \{\mathbf{p}, \mathbf{p}^*\} - i\{\mathbf{l}, \mathbf{l}^*\})$

products meet this identity.⁴⁵ We will further discuss the significance of the properties of field products in Sec. V.

The important point that Eq. (6) illustrates is that the diagrammatic calculation of the polarization grating $\{\mathbf{x}, \mathbf{y}^*\}$ can be decomposed into four intensity gratings: a right circular grating, a -45° linear grating that is spatially $\pi/2$ radians out of phase with the right circular grating, a left circular grating that is spatially π radians out of phase with the right circular grating, and a 45° linear grating that is spatially $3\pi/2$ radians out of phase with the right circular grating. This decomposition is illustrated in Fig. 4. Furthermore, this is a rigorous property of the third-order polarization (and equivalently $\chi^{(3)}$), regardless of how $\rho^{(3)}$ is derived.

The decomposed intensity-grating picture is essentially equivalent to the electric-field picture that we made for the polarization grating. Note that linearly polarized transitions

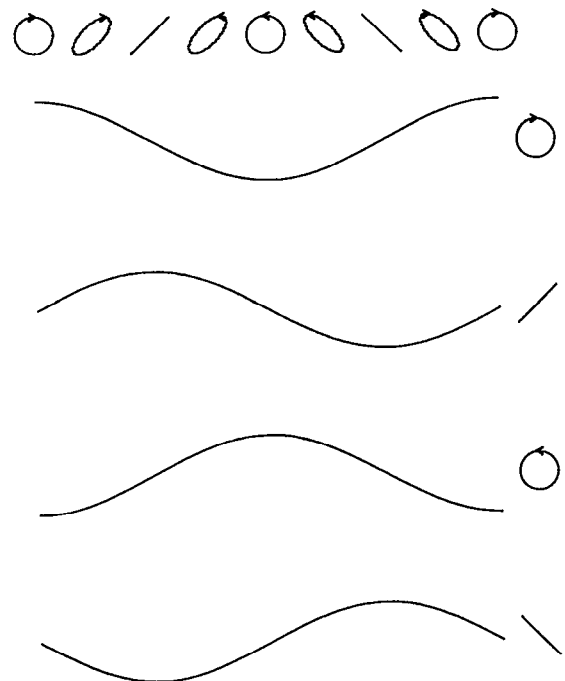


FIG. 4. Decomposition of linear polarization grating based on the GDM.

TABLE II. Polarization relationships.

Polarization (η)	Conjugate polarization	(η^*) Component polarizations
r	l	$(1/\sqrt{2})(\mathbf{x} + i\mathbf{y})$
l	r	$(1/\sqrt{2})(\mathbf{x} - i\mathbf{y})$
x	x	$(1/\sqrt{2})(\mathbf{r} + \mathbf{l})$
y	y	$(i/\sqrt{2})(\mathbf{l} - \mathbf{r})$
p	p	$(1/\sqrt{2})(\mathbf{x} + \mathbf{y})$
m	m	$(1/\sqrt{2})(\mathbf{x} - \mathbf{y})$

are driven to some extent in the predominantly circular portions of the electric-field picture and circularly polarized transitions are driven to some extent in the predominantly linear portions. Since the GDM breaks orientational gratings into separate component intensity gratings, it is ideally suited for the phenomenological inclusion of secondary grating effects such as population decay, heat deposition (thermal gratings), molecular alignment through the nuclear OKE, or even the spatial dependence of the population transfer out of various ground states. This is because each individual component intensity grating is created with two fields of the same polarization; if one knows that a particular system interacts with a particular polarization of light in a given manner, then this known interaction is modulated in strength sinusoidally as one moves along a fringe of the grating. It is therefore easy to develop, with little or no calculation, qualitative pictures of what happens in a given polarization-grating experiment. We will demonstrate in II how the GDM can give such qualitative insights.

IV. EFFECTIVE TWO-INTERACTION MATRIX ELEMENTS

DPT calculations for TG experiments must be summed over all combinations of couplings of ground- and excited-state levels (i.e., those couplings that are allowed by the laser-field frequencies and bandwidths). These summations can be quite involved. We show here that the necessary summations can be performed in advance and tabulated for a given molecule or atom, in the form of effective two-interaction matrix elements (ETIMEs). In addition, we will show in the next section that the symmetry properties of the ETIMEs can often be used to determine whether or not some of the component gratings in a decomposition will cancel.

ETIMEs are an extension of a method for simplifying higher-order wave-mixing computations that was originally introduced by Trebino and Rahn.⁴⁶ Trebino and Rahn developed a method of simplifying DPT calculations in sodium-atom experiments. They considered only Feynman diagrams in which ground-state coherences are created during the excitation steps; these are the "absorption" TG Feynman diagrams [Figs. 2(a) and 2(b) and Figs. 3(a) and 3(b)]. Here we will generalize this method, and show that a similar simplification can be made for diagrams in which excited-state coherences are created during the excitation steps [these "stimulated-emission" diagrams are in Figs. 2(c) and 2(d) and Figs. 3(c) and 3(d)].

We start by writing the terms corresponding to the TG Feynman diagrams. For the sake of clarity we write these terms with the approximation that the pulses are temporal delta functions but have finite frequency bandwidths. We also assume that the signal pulses are temporal delta functions. This is a convenient limit in which to work for time-domain calculations, and in many cases the observable signal can be modeled by calculating the basic TG signal in this manner and then convolving with the instrument-response function.⁴⁷ If the response time of the system is long compared to the pulse durations, this limit is an accurate description even without convolutions. The terms that correspond

to the Feynman diagrams [Figs. 2(a) and 2(b)] are almost identical, and are given by⁴⁷

$$\begin{aligned} \wp^{(3)}(t) \propto & E_1 E_2^* E_3 (\boldsymbol{\mu}_{bc} \cdot \boldsymbol{\eta}_1) (\boldsymbol{\mu}_{ca} \cdot \boldsymbol{\eta}_2^*) (\boldsymbol{\mu}_{ad} \cdot \boldsymbol{\eta}_3) \\ & \times (\boldsymbol{\eta}_{ab} \cdot \boldsymbol{\eta}_s^*) \exp(i\omega_{ab} t) \\ & \times \exp(-\Gamma_{ab} t) \rho_{bb(aa)}(0), \end{aligned} \quad (7a)$$

where ω_{ba} is $(E_b - E_a)/\hbar$, Γ_{ba} is the phenomenological damping constant of coherences between states $|a\rangle$ and $|b\rangle$, $\rho_{aa}(0)$ is the density-matrix element giving the normalized initial population of state $|a\rangle$, and $\boldsymbol{\mu}_{jk} \cdot \boldsymbol{\eta}_m$ is shorthand for $\langle k | \boldsymbol{\eta}_m \cdot \mathbf{r} | j \rangle$. Similarly, the terms that correspond to the Feynman diagrams in Fig. 2(c) and 2(d) are identical, and are given by⁴⁷

$$\begin{aligned} \wp^{(3)}(t) \propto & E_1 E_2^* E_3 (\boldsymbol{\mu}_{ad} \cdot \boldsymbol{\eta}_1) (\boldsymbol{\mu}_{ca} \cdot \boldsymbol{\eta}_2^*) (\boldsymbol{\mu}_{bc} \cdot \boldsymbol{\eta}_3) \\ & \times (\boldsymbol{\mu}_{ab} \cdot \boldsymbol{\eta}_s^*) \exp(i\omega_{dc} t) \\ & \times \exp(-\Gamma_{dc} t) \rho_{aa}(0). \end{aligned} \quad (7b)$$

The diagrams in Figs. 2(a) and 2(b) give identical terms in the delta-function pulse limit if $\rho_{aa}(0) = \rho_{bb}(0)$ for all $|a\rangle$ and $|b\rangle$. If $\rho_{aa}(0) \neq \rho_{bb}(0)$, the diagrams give terms that are proportional to each other in this limit. These diagrams do not give identical terms when the pulses are not temporal delta functions, and neither do the diagrams in Figs. 2(c) and 2(d). However, the methods that we present here are valid for any TG calculation.

The total third-order polarization is derived by summing Eqs. (7a) and (7b) over all relevant states $|a\rangle$, $|b\rangle$, $|c\rangle$, and $|d\rangle$ (and by doing whatever orientational averaging is necessary, which will not be considered for the moment). Note, however, that in Eq. (7a) the states $|c\rangle$ and $|d\rangle$ appear only in the transition-dipole matrix elements; similarly, in Eq. (7b) the states $|a\rangle$ and $|b\rangle$ appear only in the transition-dipole matrix elements. Thus we can perform the summations over these states in advance. Ignoring the density-matrix elements for the moment, the total contributions to $\wp^{(3)}$ from the absorption and stimulated-emission diagrams are given by

$$\begin{aligned} \wp^{(3)}(\text{abs}) \propto & E_1 E_2^* E_3 \sum_a \sum_b \left[\sum_c (\boldsymbol{\mu}_{bc} \cdot \boldsymbol{\eta}_1) (\boldsymbol{\mu}_{ca} \cdot \boldsymbol{\eta}_2^*) \right] \\ & \times \left[\sum_d (\boldsymbol{\mu}_{ad} \cdot \boldsymbol{\eta}_3) (\boldsymbol{\mu}_{db} \cdot \boldsymbol{\eta}_s^*) \right] \\ & \times \exp(i\omega_{ab} t) \exp(-\Gamma_{ab} t), \end{aligned} \quad (8a)$$

and

$$\begin{aligned} \wp^{(3)}(\text{em}) \propto & E_1 E_2^* E_3 \sum_c \sum_d \left[\sum_a (\boldsymbol{\mu}_{ad} \cdot \boldsymbol{\eta}_1) (\boldsymbol{\mu}_{ca} \cdot \boldsymbol{\eta}_2^*) \right] \\ & \times \left[\sum_b (\boldsymbol{\mu}_{bc} \cdot \boldsymbol{\eta}_3) (\boldsymbol{\mu}_{db} \cdot \boldsymbol{\eta}_s^*) \right] \\ & \times \exp(i\omega_{dc} t) \exp(-\Gamma_{dc} t). \end{aligned} \quad (8b)$$

The quantities inside the first and second sets of brackets in Eq. (8a) represent interactions that couple the ground-state manifold to the states $|c\rangle$ and the states $|d\rangle$, respectively, whether $|c\rangle$ and $|d\rangle$ are in the same or in different excited-state manifolds. We perform the summations inside each set of brackets and rewrite the equation in the form

$$\rho^{(3)}(\text{abs}) \propto E_1 E_2^* E_3 \sum_{a,b} [{}^c M_{ba}(\eta_1, \eta_2) {}^d M_{ab}(\eta_3, \eta_s) \\ \times \exp(i\omega_{ab}t) \exp(-\Gamma_{ab}t)], \quad (9a)$$

where the ${}^{\text{ex}}M_{ab}(\eta_j, \eta_k)$ are the absorption effective two-interaction matrix elements (*a*-ETIMES). ${}^{\text{ex}}M_{ab}(\eta_j, \eta_k)$ is the sum of products of matrix elements that couple states $|a\rangle$ and $|b\rangle$ (which are in the same ground-state manifold) through excited-state manifold (*ex*) by absorption at polarization η_j and stimulated emission at polarization η_k^* . Similarly, we can write for the stimulated-emission Feynman diagrams,

$$\rho^{(3)}(\text{em}) \propto E_1 E_2^* E_3 \sum_{c,d} [{}_a M_{dc}(\eta_1, \eta_2) {}_b M_{cd}(\eta_3, \eta_3) \\ \times \exp(i\omega_{dc}t) \exp(-\Gamma_{dc}t)], \quad (9b)$$

where the ${}_{\text{gr}}M_{cd}(\eta_j, \eta_k)$ are the stimulated-emission effective two-interaction matrix elements (*e*-ETIMES). ${}_{\text{gr}}M_{cd}(\eta_j, \eta_k)$ is the sum of products of matrix elements that couple states $|c\rangle$ and $|d\rangle$ (which are in the same excited-state manifold) through "ground"-state manifold (*gr*) by absorption at polarization η_j and at polarization η_k^* . Note that to differentiate between the two types of ETIMES, for *a*-ETIMES we place the relevant excited-state manifold in a superscript and for *e*-ETIMES we place the relevant ground-state manifold in a subscript.

We must be somewhat careful in our definition of the ETIMES. For instance, an *a*-ETIME ${}^c M_{ab}(\eta_j, \eta_k)$ implies closure over states $|c\rangle$; i.e., we must consider all states $|c\rangle$ that are within the laser frequency bandwidth. If the bandwidth of the laser is smaller than the width of an excited-state manifold, then only those states within the bandwidth should be considered. In addition, we must reintroduce the density-matrix elements to take into account the initial populations of the ground-state levels. For the diagrams in Figs. 2(a) and 2(b), we multiply the summand in Eq. (9a) by $\rho_{bb}(0)$ and $\rho_{aa}(0)$, respectively. We must treat Eq. (9b) somewhat differently, since the initial states have already been summed over; a factor of $\rho_{aa}(0)$ should have been included in the summation over states $|a\rangle$ in Eq. (8b). To take care of this problem, the first (but not the second) *e*-ETIME in Eq. (9b) must include this weighting; since thermal equilibrium is responsible for the differences in the initial populations of the states $|a\rangle$, we can think of the first *e*-ETIME in Eq. (9b) as being temperature dependent.

The power of ETIMES is that they can be calculated once and tabulated for a given atom or molecule. ETIMES thus save considerable calculational time, because all two-interaction pathways that couple a given pair of states are summed over in advance. In fact, for molecules it usually suffices to tabulate ETIMES for a single linear polarization (within a given laser frequency bandwidth range and at a given temperature).

V. NONCONTRIBUTING GRATINGS

The symmetry properties of $\chi^{(3)}$ are known for all space groups.⁴⁸ By considering these symmetry properties, it is often possible to prove that the contributions to $\rho^{(3)}$ of two intensity gratings in a decomposition must cancel one an-

other, and therefore that the gratings need not be considered in the calculation. Here we consider what happens in isotropic systems, but a similar procedure can be used for any space group.

In isotropic systems, $\chi_{xyxy} = \chi_{yxyx}$ (we drop the superscript of $\chi^{(3)}$ when it has subscripts that are indicative of four electric fields). For anything other than a two-level system, $\rho^{(3)}$ contains terms that oscillate at different frequencies. The above relation must hold for all terms in $\chi^{(3)}$ that oscillate at a given frequency. Consider, for instance, an atom or molecule with some number of degenerate ground states $|a\rangle$ and some number of degenerate ground states $|b\rangle$, where $E_a \neq E_b$. Because the sum of the terms that oscillate at ω_{ba} in χ_{xyxy} must be equal to the sum of the terms in χ_{yxyx} that oscillate at this frequency, we require that

$$\sum_a \sum_b {}^c M_{ab}(\mathbf{x}, \mathbf{y}) {}^d M_{ba}(\mathbf{x}, \mathbf{y}) \\ = \sum_a \sum_b {}^c M_{ab}(\mathbf{y}, \mathbf{x}) {}^d M_{ba}(\mathbf{y}, \mathbf{x}). \quad (10)$$

$\rho^{(3)}$ contains many terms such as these that must be equal, both for the absorption diagrams and for the stimulated-emission diagrams. These expressions cannot, in general, be broken down any further. However, there are two important special cases for which they can be simplified: $M_{pq}(\mathbf{x}, \mathbf{y}) = M_{pq}(\mathbf{y}, \mathbf{x})$ and $M_{pq}(\mathbf{x}, \mathbf{y}) = -M_{pq}(\mathbf{y}, \mathbf{x})$. Note that these are not specifically *a*-ETIMES or *e*-ETIMES; this notation is intended to indicate that, for the special case to hold, these relationships must hold for *all* relevant ETIMES.

In each of these two cases the problem can, in some sense, be broken down and considered two fields at a time. Thus, we can rewrite the two cases in field product notation as $\{\mathbf{x}, \mathbf{y}^*\} = \{\mathbf{y}, \mathbf{x}^*\}$ and $\{\mathbf{x}, \mathbf{y}^*\} = -\{\mathbf{y}, \mathbf{x}^*\}$. The full import of these two relations can be seen once we write the decompositions for $\{\mathbf{x}, \mathbf{y}^*\}$ and $\{\mathbf{y}, \mathbf{x}^*\}$,

$$\{\mathbf{x}, \mathbf{y}^*\} = (i/2) (\{ \mathbf{r}, \mathbf{r}^* \} + i \{ \mathbf{m}, \mathbf{m}^* \} \\ - \{ \mathbf{l}, \mathbf{l}^* \} - i \{ \mathbf{p}, \mathbf{p}^* \}), \quad (11a)$$

and

$$\{\mathbf{y}, \mathbf{x}^*\} = (i/2) (\{ \mathbf{l}, \mathbf{l}^* \} + i \{ \mathbf{m}, \mathbf{m}^* \} \\ - \{ \mathbf{r}, \mathbf{r}^* \} - i \{ \mathbf{p}, \mathbf{p}^* \}). \quad (11b)$$

From these equations, we see that when $\{\mathbf{x}, \mathbf{y}^*\} = \{\mathbf{y}, \mathbf{x}^*\}$, $\{ \mathbf{r}, \mathbf{r}^* \} = \{ \mathbf{l}, \mathbf{l}^* \}$, and therefore the contributions to $\rho^{(3)}$ from the circularly polarized component intensity gratings cancel one another. Similarly, when $\{\mathbf{x}, \mathbf{y}^*\} = -\{\mathbf{y}, \mathbf{x}^*\}$, the contributions from the linearly polarized component gratings cancel one another.

The relation $\chi_{xyxy} = \chi_{yxyx}$ is true for many space groups,⁴⁸ so this result extends beyond isotropic systems. We show here that all isotropic molecular systems fall into the first special case so long as only absorption and stimulated emission need be considered (as opposed to effects such as circular dichroism). Consider a pair of molecular states $|j\rangle$ and $|k\rangle$ that are coherently coupled by a pair of transitions that share a common ground or excited state $|l\rangle$. There is some arbitrary angle α between the dipole moments of these transitions. We label the transition-dipole moments \mathbf{j} and \mathbf{k} ,

and we consider coherences at frequency ω_{jk} . If the first excitation beam is x polarized and the second excitation beam is y polarized, then the contribution of this pair of transitions to the ETIME for coherences at ω_{jk} is obtained by performing a double average. We average the product of the x projection of \mathbf{j} and the y projection of \mathbf{k} over all possible vectors \mathbf{j} and over all vectors \mathbf{k} that make an angle α with each \mathbf{j} .

We can perform a similar procedure if the first excitation beam is y polarized and the second x polarized; this set of averages must give the same result as the first. This can be seen through a simple counting argument. For a particular pair of vectors \mathbf{j} and \mathbf{k} separated by angle α , we define the quantity $q(\mathbf{j},\mathbf{k})$ as the product of the x projection of \mathbf{j} and the y projection of \mathbf{k} . Now we can interchange the directions of the two vectors, such that \mathbf{j}' points along \mathbf{k} and \mathbf{k}' points along \mathbf{j} . Then it must be true that $q(\mathbf{j}',\mathbf{k}') = q(\mathbf{j},\mathbf{k})$, as is illustrated in two dimensions in Fig. 5. Thus, for every pair of vectors in the $\{\mathbf{x},\mathbf{y}^*\}$ average, there is a pair of vectors in the $\{\mathbf{y},\mathbf{x}^*\}$ average that gives the same contribution. Since the choice of \mathbf{j} and \mathbf{k} was arbitrary, it follows that, for all of the ETIMES for the system, $M_{jk}(\mathbf{x},\mathbf{y}) = M_{jk}(\mathbf{y},\mathbf{x})$ (or, equivalently, $\{\mathbf{x},\mathbf{y}^*\} = \{\mathbf{y},\mathbf{x}^*\}$). This condition implies that only the linear component gratings in the decomposition contribute to the signal.

Although molecules have well-defined transition-dipole moment directions, atoms do not. Thus, isotropic atomic systems do not necessarily meet the condition $\{\mathbf{x},\mathbf{y}^*\} = \{\mathbf{y},\mathbf{x}^*\}$; the ETIMES must be calculated separately for each set of atomic transitions. Many isotropic atomic systems do fall under one or the other of these special cases, however. As we will discuss in II, the a -ETIMES for the sodium D_1 and D_2 transitions fall under the latter special case, $\{\mathbf{x},\mathbf{y}^*\} = -\{\mathbf{y},\mathbf{x}^*\}$, as do the e -ETIMES for the D_1 transitions. However, the e -ETIMES for the D_2 transitions conform to neither of these special cases.

Thus, for most linear polarization-grating calculations, only two of the four component intensity gratings need to be

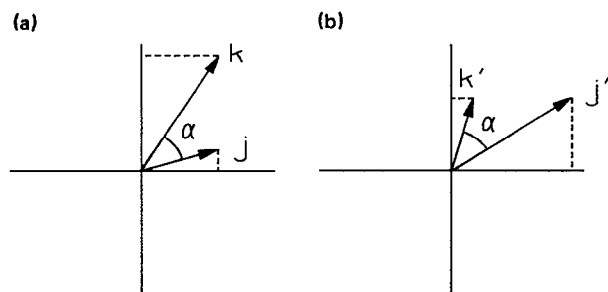


FIG. 5. Two-dimensional depiction of argument that $\{\mathbf{x},\mathbf{y}^*\} = \{\mathbf{y},\mathbf{x}^*\}$ in isotropic molecular liquids in which absorption and emission are the only important effects. To calculate the field product $\{\mathbf{x},\mathbf{y}^*\}$ for two transition dipole moments \mathbf{j} and \mathbf{k} that are separated by angle α , the absolute value of the x projection of \mathbf{j} times the absolute value of the y projection of \mathbf{k} is averaged over all possible orientations of the \mathbf{j} and \mathbf{k} . The polarizations are switched to calculate $\{\mathbf{y},\mathbf{x}^*\}$. However, for every term in the first average (a), there is an identical term in the second average that is obtained by interchanging the directions of the vectors (b). Thus the field products are equal.

considered. Furthermore, because the two gratings that are considered are either both linearly polarized or both circularly polarized, the calculation for one must be related to the calculation for the other. This relationship is easy to derive in most cases, and so the GDM calculation involves calculating in detail the contribution to $\rho^{(3)}$ of only one of the four-component intensity gratings. Even when all four component gratings contribute to the signal, the GDM provides the spatial information necessary for including secondary effects and for understanding the nature of decay constants. In addition, the ETIMES simplify in the perturbative calculation even if it is performed without decomposition.

VI. CONCLUSIONS

Electric-field pictures and DPT are both useful methods for understanding orientational gratings, but each has drawbacks; the former provides insight but little calculational power, while the latter provides calculational power but often little insight. We have introduced a new way to view orientational gratings, based on the fact that it is possible to decompose any orientational grating into a sum of intensity gratings, each of which acts as if it was created by two beams of identical polarizations. These component gratings correspond to the electric-field pictures, in that, for instance, the maximum of the right circularly polarized (RCP) grating in the linear polarization grating decomposition is where RCP appears in the electric-field picture for this grating. Thus, the GDM makes a rigorous connection between electric-field pictures and perturbative calculations. With use of the GDM, it is possible to understand the spatial dependences in orientational gratings, thereby providing a means of including secondary effects in grating calculations. We have also introduced ETIMES as a method of simplifying grating calculations by performing many of the necessary summations in advance. By considering the symmetry properties of $\chi^{(3)}$ and of the ETIMES for a particular system, it is often possible to show that pairs of gratings in a decomposition have canceling contributions to $\rho^{(3)}$, thus further simplifying the GDM calculation.

In the following paper, we demonstrate the application of the GDM to two different problems, nuclear optical Kerr effect orientational gratings and gratings of gas-phase sodium atoms. We will show how the GDM can simplify and provide insight into orientational grating calculations.

ACKNOWLEDGMENTS

This work was supported in part by the Office of Naval Research, Physics Division, Grant No. N000014-89-J1119. R.T. thanks the U.S. Department of Energy, Office of Basic Energy Sciences, Chemical Sciences Division, for support. J.T.F. thanks the National Science Foundation for a graduate fellowship. We wish to thank Dr. Mark Dugan, Dr. Ed Quitevas, and Dr. Ad Kostenbauder for critical readings.

¹M. D. Levenson and S. S. Kano, *Introduction to Nonlinear Laser Spectroscopy* (Academic, Boston, 1988).

²Y. R. Shen, *The Principles of Nonlinear Optics* (Wiley-Interscience, New York, 1984).

- ¹H. J. Eichler, P. Günter, and D. W. Pohl, *Laser-Induced Dynamic Gratings* (Springer-Verlag, Berlin, 1986).
- ²T. R. Rose, W. L. Wilson, G. Wäckerle, and M. D. Fayer, *J. Phys. Chem.* **91**, 1704 (1987).
- ³T. S. Rose, W. L. Wilson, G. Wäckerle, and M. D. Fayer, *J. Chem. Phys.* **86**, 5370 (1987).
- ⁴J. T. Fourkas, T. R. Brewer, H. Kim, and M. D. Fayer, *Opt. Lett.* **16**, 177 (1991).
- ⁵J. T. Fourkas, T. R. Brewer, H. Kim, and M. D. Fayer, *J. Chem. Phys.* **95**, 5775 (1991).
- ⁶D. W. Phillion, D. J. Kuizenga, and A. E. Siegman, *Appl. Phys. Lett.* **27**, 85 (1975).
- ⁷F. Rondelez, H. Hervet, and W. Urbach, *Chem. Phys. Lett.* **53**, 138 (1978).
- ⁸P. D. Hyde, T. E. Evert, and M. D. Ediger, *J. Chem. Phys.* **93**, 2274 (1990).
- ⁹S. Ruhman, B. Kohler, A. G. Joly, and K. A. Nelson, *Chem. Phys. Lett.* **141**, 16 (1987).
- ¹⁰G. A. Kenney-Wallace and S. Wallace, *IEEE J. Quantum Electron.* **QE-19**, 719 (1983).
- ¹¹W. Urbach, H. Hervet, and F. Rondelez, *Mol. Cryst. Liq. Cryst.* **46**, 209 (1978).
- ¹²F. W. Deeg and M. D. Fayer, *J. Chem. Phys.* **91**, 2269 (1989).
- ¹³L. B. Au, H. Eichler, R. Macdonald, and L. Solymar, *Proceedings of Non-linear Optics: Materials, Phenomena, and Devices*, edited by H. M. Gibbs, D. G. Steel, J. F. Lam, and P. Yeh (Optical Society of America, Washington, D.C., 1990).
- ¹⁴Y. Aoyagi, Y. Segawa, and S. Namba, *IEEE J. Quantum Electron.* **QE-22**, 1320 (1986).
- ¹⁵T. S. Rose, *Chem. Phys. Lett.* **106**, 13 (1984).
- ¹⁶J. R. Salcedo and A. E. Siegman, *IEEE J. Quantum Electron.* **QE-15**, 250 (1979).
- ¹⁷M. D. Fayer, *IEEE J. Quantum Electron.* **QE-22**, 1437 (1986).
- ¹⁸J. M. Brown, L. J. Slutsky, K. A. Nelson, and L.-P. Cheng, *J. Geophys. Res.* **94**, 9485 (1989).
- ¹⁹J. J. Kasinski, L. Gomez-Jahn, K. J. Leong, S. M. Gracewski, and R. J. D. Miller, *Opt. Lett.* **13**, 710 (1988).
- ²⁰J. J. Kasinski, L. Gomez-Jahn, L. Min, Q. Bao, and R. J. D. Miller, *J. Lumin.* **40-41**, 555 (1988).
- ²¹D. P. Norwood *et al.*, in *Ultrafast Phenomena VII*, edited by C. B. Harris, E. P. Ippen, G. A. Mourou, and A. H. Zewail (Springer-Verlag, Berlin, 1990).
- ²²M. R. Farrar, L.-T. Cheng, Y.-X. Ya, and K. A. Nelson, *IEEE J. Quantum Electron.* **QE-22**, 1453 (1986).
- ²³M. B. Ritter, D. D. Awschalom, and M. W. Schafer, *Phys. Rev. Lett.* **61**, 966 (1988).
- ²⁴J. J. Kasinski, L. A. Gomez-Jahn, K. J. Faran, S. M. Gracewski, and R. J. D. Miller, *J. Chem. Phys.* **90**, 1253 (1989).
- ²⁵A. von Jena and H. E. Lessing, *Opt. Quantum Electron.* **11**, 419 (1979).
- ²⁶T. F. Boggess, A. L. Smirl, and B. S. Wherrett, *Opt. Commun.* **43**, 128 (1982).
- ²⁷B. S. Wherrett, A. L. Smirl, and T. F. Boggess, *IEEE J. Quantum Electron.* **QE-19**, 680 (1983).
- ²⁸A. L. Smirl, T. F. Boggess, B. S. Wherrett, G. P. Perryman, and A. Miller, *IEEE J. Quantum Electron.* **QE-19**, 690 (1983).
- ²⁹D. Kühnke, *Appl. Phys. B* **34**, 129 (1984).
- ³⁰G. Eyring and M. D. Fayer, *J. Chem. Phys.* **81**, 4314 (1984).
- ³¹R. Trebino, C. E. Barker, and A. E. Siegman, *IEEE J. Quantum Electron.* **QE-22**, 1413 (1986).
- ³²L. J. Rothberg and N. Bloembergen, *Phys. Rev. A* **30**, 820 (1984).
- ³³T. K. Yee and T. K. Gustafson, *Phys. Rev. A* **18**, 1597 (1978).
- ³⁴Y. Prior, *IEEE J. Quantum Electron.* **QE-22**, 37 (1984).
- ³⁵J. Bordé and C. J. Bordé, *J. Mol. Spectrosc.* **78**, 353 (1979).
- ³⁶J. G. Fujimoto and T. K. Yee, *IEEE J. Quantum Electron.* **QE-19**, 861 (1983).
- ³⁷J. G. Fujimoto and T. K. Yee, *IEEE J. Quantum Electron.* **QE-22**, 1215 (1986).
- ³⁸P. Ye and Y. R. Shen, *Phys. Rev. A* **25**, 2183 (1982).
- ³⁹S. Mukamel and R. F. Loring, *J. Opt. Soc. Am. B* **3**, 595 (1986).
- ⁴⁰J. T. Fourkas, R. Trebino, and M. D. Fayer, *J. Chem. Phys.* **97**, 78 (1992), following paper.
- ⁴¹D. D. Diott, *Annu. Rev. Phys. Chem.* **37**, 157 (1986).
- ⁴²N. Young, *An Introduction to Hilbert Space* (Cambridge University, Cambridge, 1988).
- ⁴³R. D. Richtmyer, *Principles of Advanced Mathematical Physics*, Vol. 1 (Springer-Verlag, Berlin, 1978).
- ⁴⁴R. Trebino and L. A. Rahn, *Opt. Lett.* **12**, 912 (1987).
- ⁴⁵J. T. Fourkas, Ph. D. thesis, Stanford University, 1991 (unpublished).
- ⁴⁶R. W. Hellwarth, *Prog. Quantum Electron.* **5**, 1 (1977).